PROCEEDINGS, 43rd Workshop on Geothermal Reservoir Engineering
Stanford University, Stanford, California, February 12-14, 2018
SGP-TR-213

Volcanic Texture Identification and Influence on Permeability Using a Borehole Resistivity Image Log in the Whakamaru Group ignimbrite, Wairakei Geothermal Field, New Zealand

Sarah D. Milicich[1], Cécile Massiot[1], David D. McNamara[2]

[1]GNS Science, 1 Fairway Drive, Avalon, Lower Hutt, 5010, New Zealand

[2]Department of Earth and Ocean Sciences, National University of Ireland, Galway

s.milicich@gns.cri.nz

Keywords: Borehole Resistivity Image Log, Wairakei, Permeability, Volcanic Fabric, New Zealand.

ABSTRACT

Discerning the contributions to fluid flow in a geothermal reservoir from intrinsic and structural permeability components is an important, yet difficult task. High-quality, resistivity borehole image log data (Formation MicroImager; FMI) collected from the Whakamaru Group ignimbrite in well WK271, Wairakei Geothermal Field, New Zealand, has been used to investigate the textural characteristics of volcanic rocks in the geothermal reservoir, with a view to improving reservoir model inputs. Textural analysis of the FMI log in the Whakamaru Group ignimbrite was able to provide an improved internal stratigraphy compared to that derived solely from drill-cuttings, and offers insights into the volcanic processes that generated it. Based on volcanic textures identified on the WK271 FMI image log, seven individual flow units in the Whakamaru Group ignimbrite are recognized, and are separated by texturally characteristic intervals of airfall tephra. Comparison of fracture density and rock type (including welding intensity) shows a low fracture density in non-welded ignimbrites and tuff beds. The logged interval occurs over a fault zone where permeability has previously been inferred to be strongly influenced by fractures, precluding an accurate assessment of the ignimbrites intrinsic permeability.

1. INTRODUCTION

Permeability of volcaniclastic formations in geothermal reservoirs is typically controlled by a mixture of fractures and matrix (Grant and Bixley, 2011), with the fracture component generally increasing with depth and bulk density. Characterizing the contribution of both fracture and matrix to permeability is important for field management, reservoir modelling, and for better understanding of the reservoir for future well siting (Bignall et al., 2010).

Borehole image logs are commonly used as a tool for subsurface structure and stress field characterization and the identification of where structurally controlled fluid flow occurs in geothermal fields, in New Zealand (McNamara and Massiot, 2016; McNamara et al., 2017; Massiot et al., 2017) and overseas (e.g., Genter et al., 1997; Davatzes and Hickman, 2009; Davatzes and Hickman, 2010; Batir et al., 2012). However, borehole image logs can also directly reveal geological formation textures and fabrics (Bartetzko et al., 2003; Davatzes and Hickman, 2005; Halwa et al., 2013; Watton et al., 2014), with resistivity image logs reportedly advantageous over acoustic image logs for this purpose due to higher contrast of lithological components (Davatzes and Hickman, 2005). So, while structure and stress analyses of borehole image logs in geothermal systems hosted in volcanic rocks is now commonly undertaken, volcanological interpretation of rocks from resistivity logs is rarely reported (though they are more commonly used in oil and gas settings, e.g., Watton et al., 2014).

Resistivity images are infrequently acquired in New Zealand geothermal wells due to the high borehole temperatures, which exceed traditional tool limitations (~175°C). However, when a borehole can be cooled to <150°C via quenching, resistivity image logs (in current study the Schlumberger Formation MicroImager - FMI) can be acquired; this has been reported only once before in New Zealand from the Ngatamariki Geothermal Field (Halwa et al., 2013). This paper provides preliminary observations of lithological textures and fabrics in an important geothermal reservoir, the Whakamaru Group ignimbrite, in the Wairakei Geothermal Field, using an FMI log in well WK271 (Figure 1). From this dataset insight into the processes that deposited this unit, and the potential contribution to geothermal fluid flow from intrinsic permeability are investigated.

1.1 Geological setting

The Wairakei Geothermal Field (348 MWe installed capacity) is located in the Taupo Volcanic Zone (TVZ) in New Zealand (Figure 1), which represents the active, southern portion of the Lau-Havre-Taupo extensional back arc basin, formed as a result of westward subduction of the Pacific Plate beneath the North Island (Begg and Mouslopoulou, 2010; Wilson and Rowland, 2016). The TVZ is the locus of intense silicic volcanic activity during the last ~2 Ma, with multiple ignimbrites sourced from eight calderas (Figure 1; Wilson and Rowland, 2016). The shallow geology (above ~600 m) of the Wairakei area consists of sediments, lavas, and volcaniclastic deposits <220 ka and deeper geology consists of a succession of pyroclastic deposits, reworked equivalents, lavas, and sedimentary units (Grindley, 1960; Rosenberg et al., 2009; Bignall et al., 2010; Rosenberg, 2017). These geological units are variably hydrothermally altered, generally following a trend of increasing rank and intensity with depth (Bignall et al., 2010).

Existing analyses of borehole image data from the Wairakei Geothermal Field, including the well studied in this work (WK271), indicate structural orientations are dominated by the main NE-SW regional strike trend, with sub-populations of E-W, and N-S strikes (McLean and McNamara, 2011; Massiot et al., 2013; McNamara et al., 2016; Massiot et al., 2017).

The Whakamaru Group ignimbrites (WGI, Wilson et al., 1986; Brown et al., 1998; Leonard et al., 2010) are a key stratigraphic marker through the TVZ geothermal fields, and were erupted in association with collapse of the Whakamaru Caldera (Figure 1) between 349 ± 4 ka to 339 ± 5 ka (Downs et al., 2014). Different flow and fall units have been mapped at the surface and subsurface in several geothermal fields using outcrop and cuttings description complemented by rare cores, respectively (Grindley, 1960; Healy et al., 1964; Martin, 1965; Browne, 1971; Briggs, 1976; Leonard et al., 2010; Eastwood et al., 2013), but have not yet been able to be characterized using borehole logging.

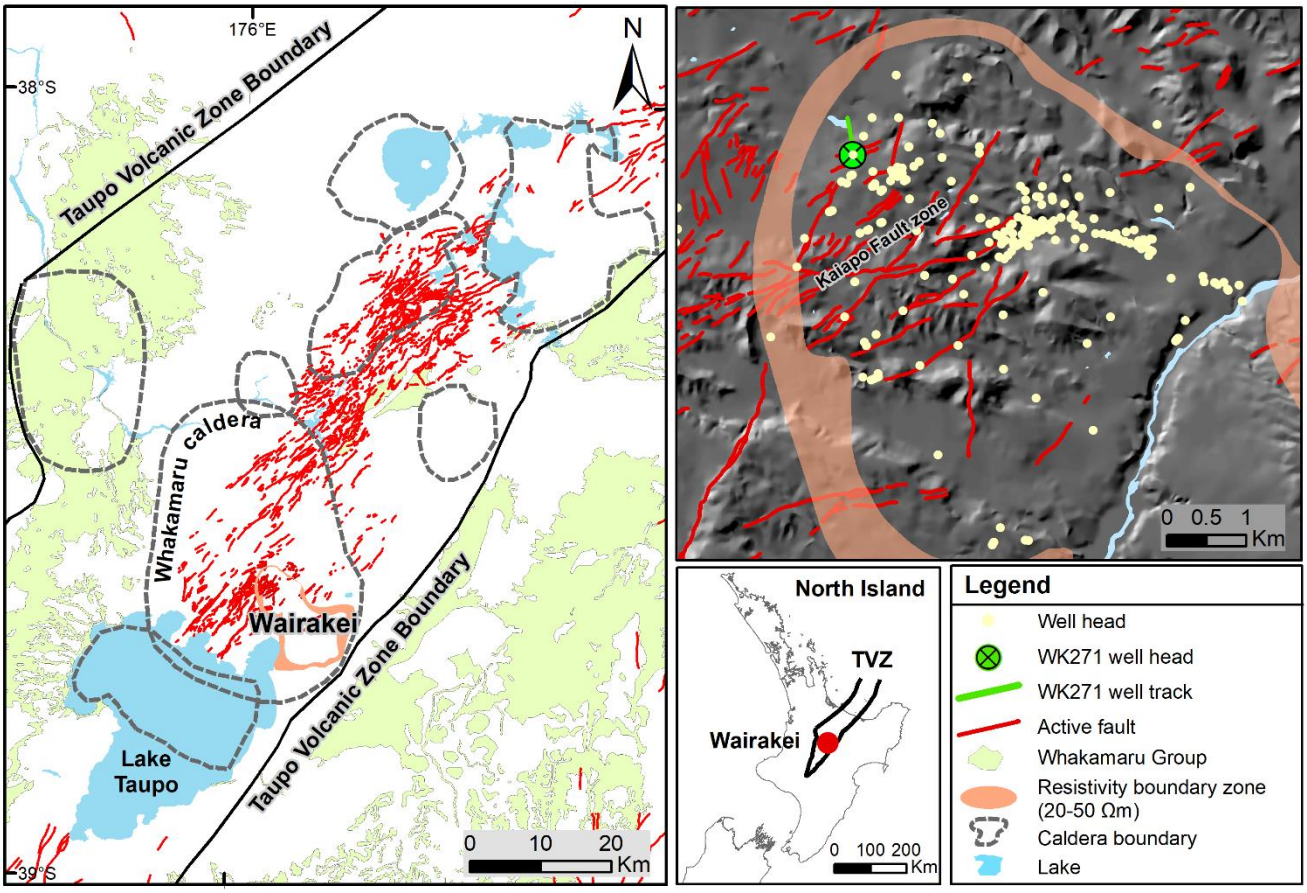

Figure 1: Location of the Wairakei Geothermal Field in relation to the Taupo Volcanic Zone (TVZ; Wilson et al., 1995), caldera boundaries (Wilson et al., 1995), mapped active faults (Langridge et al., 2016) and surface extent of the Whakamaru Group (Leonard et al., 2010). The resistivity boundary of the Wairakei Geothermal Field is delineated by 20-50 Ωm (Risk et al., 1984).

2. DATA AND METHODOLOGY

Well WK271 (Figure 1) was drilled in 2013 to a depth of -1675 mRL (meters with respect to sea level), cased to -670 mRL and is deviated ~20° towards NNW (average well inclination 20° ± 1°, average well azimuth 348° ± 2°). Resistivity image logs span the entire open-hole section (-674 to -1559 mRL). This study focusses on fracture and lithological examination of the WGI, which accounts for a 377 m-long imaged interval in well WK271.

FMI logs were processed, quality-checked, and interpreted following the workflow presented in Massiot et al. (2015). All orientations are with reference to geographic north. Lithological analysis was performed on the image log to identify texture and layering features, with care taken to differentiate these from natural fractures and stress-induced features. Fractures identified on the imaged interval follow the classification and interpretation from Massiot et al. (2017). To account the under-sampling of sinusoidal features oriented sub-parallel to the borehole, all dip data have been corrected for sampling bias according to the method outlined by Terzaghi (1965) and Massiot et al. (2015). This sampling bias if very limited for geological layers identified in well WK271 because they are dominantly dipping <40° from horizontal, intersecting the borehole dipping 70° from horizontal.

To identify azimuthal trends through the succession, depositional data is plotted as a cumulative dip-azimuth vector plot (Hurley, 1994). In this study, the plot is effectively a cross-plot of azimuth against sample number (picked dip). It is constructed by plotting the azimuth

direction as an arrow of arbitrary length for the picked dip at the bottom of the interpreted interval. The azimuth of the next picked dip above that is then plotted as another arrow, appended to that of the bottom depth, and so on up to the top of the interpreted interval.

3. RESULTS: IMAGE ANALYSIS

3.1 Lithology

The geological terminology used in this study is provided in Figure 2. The image response of lithofacies identified within the WGI has been compared with core textures from ignimbrite units of the TVZ and elsewhere, or where core is unavailable, against interpreted outcrop analogues (Figure 3). The resistivity characteristics of the FMI image through the WGI indicates there are five dominant lithofacies: non-welded ignimbrite, partially-welded ignimbrite, welded ignimbrite, tuff beds, and breccia (Figure 3).

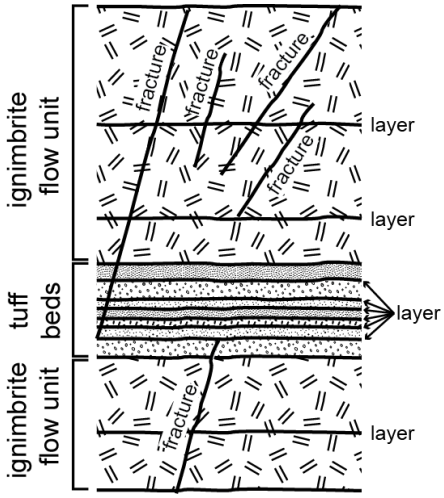

Figure 2: Sequence of tuffs and consolidated pyroclastic rocks illustrating geological terminology used in this study. Pyroclastic rocks consist of beds of ignimbrite with visible layering. Ignimbrite is a volcanic rock formed by widespread deposition and consolidation of ash flows and volcanic ejecta, which includes welded tuff and non-welded but recrystallised/lithified ash flows. "Layer" refers to the internal layering in an ignimbrite or the contact between tuff beds. "Fracture" designates a discordant feature that forms a break in the rock formation.

Within the WGI, distinct bedding and various textures are visible (Figure 3.1 to 3.8). The textures are interpreted as fiamme (ignimbrite welding texture; Figure 3.2), and breccia (Figure 3.6), along with a range in grain size sorting and degree of sorting. Some features attributed as layers may be bedding-parallel cooling joints, but cannot be differentiated and have been included as layers. These are consistent with our direct observation of drill-cuttings from Wairakei wells. Similar rock fabrics in comparable lithologies have been described on FMI logs in the nearby Ngatamariki Geothermal Field (Halwa et al., 2013).

Variations in the rock fabric within the ignimbrite have allowed it to be subdivided into non-, partially- and welded ignimbrite. The non-welded zones (Figure 3.1) contain large pumice and lithics. The partially-welded zones (Figures 3.3 & 3.4) have pumice of varying sizes, with only those < 5 cm showing thickness-width aspect ratios consistent with welding-induced flattening. Zones of welded ignimbrite (Figure 3.2) have clear fiamme-like (eutaxitic) texture formed from dense, flattened pumice. Ignimbrite flow units are delineated by tuff beds with closely spaced layers (Figure 3.7 & 3.8). There are clear variations in grain size and abundance of both pumice and lithics within the intervals interpreted as ignimbrite flow units. Along with overall variations, there are also zones of coarse textured breccia (Figure 3.6), which may represent material segregated in the pyroclastic density currents that deposited the ignimbrite (Branney and Kokelaar, 2002). Tuff beds show varying thickness, and in places cross-cutting relationships (Figures 3.5, 3.7 & 3.8).

3.2 Layering orientation

The interpreted interval lies between the upper contact of the WGI with the Waiora Formation at -936.8 mRL and the basal contact of the WGI with the Tahorakuri Formation at -1288.4 mRL. In the WGI 303 geological layers were identified. Of the geological layers, 82 were layers within ignimbrite flow units and 201 were layers in bedding intervals between ignimbrite flow units.

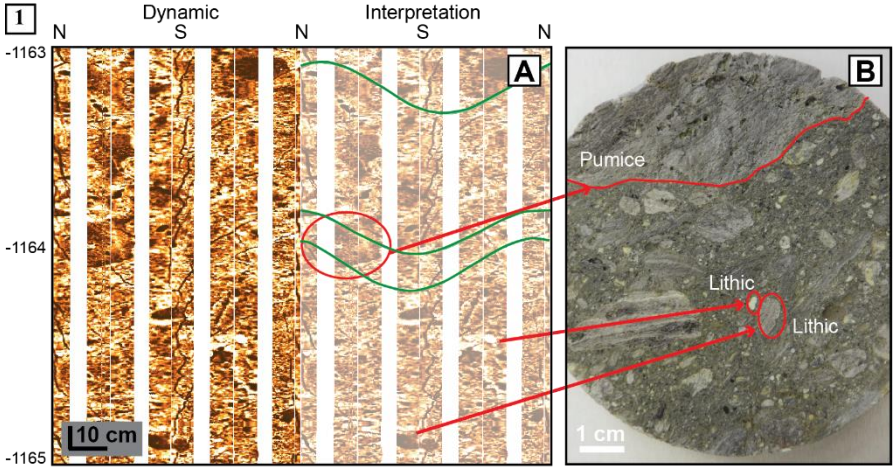

A: FMI image log with low resistivity fractures (green sinusoids). Non-welded ignimbrite. Lithics (high and low resistivity) and pumice clasts are common.
B: Core of representative non-welded ignimbrite (Ahuroa Ignimbrite, Arapuni Dam).

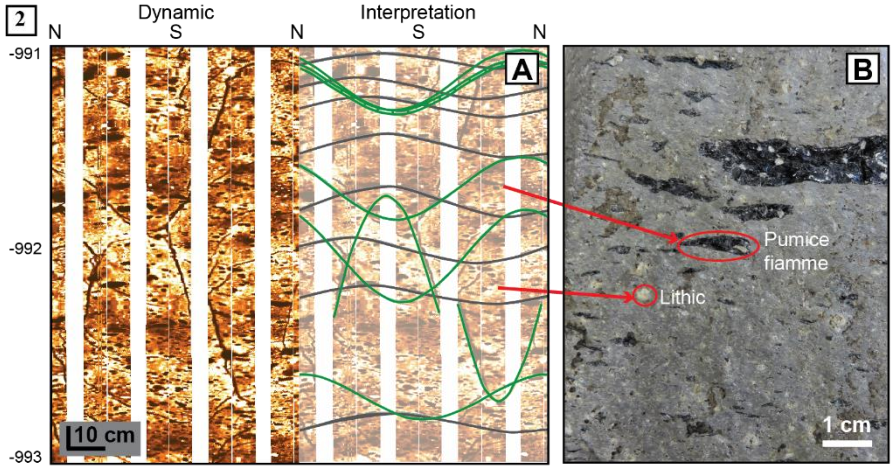

A: FMI image log with low resistivity fractures (green sinusoids) and layers (grey sinusoids). Welded ignimbrite with pumice fiamme (low resistivity) and lithics (high resistivity).
B: Core of representative welded ignimbrite (Mamaku Ignimbrite, Tokoroa).

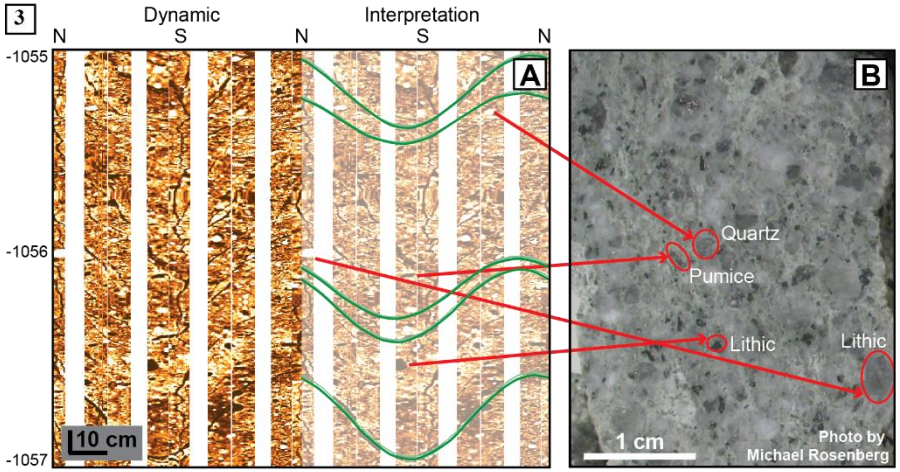

A: FMI image log with low resistivity fractures (green sinusoids). Partially-welded ignimbrite. Only small pumice (low resistivity) show any degree of flattening. Lithics are both high and low resisitvity. Quartz crystals are common (high resistivity)
B: Core of partially-welded Whakamaru Group ignimbrite in well WK121 (Wairakei Geothermal Field).

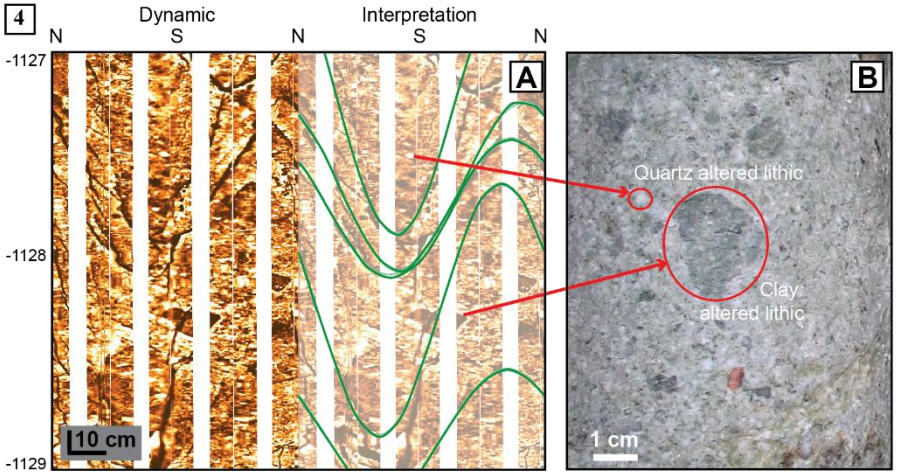

A: FMI image log with low resistivity fractures (green sinusoids). Partially-welded ignimbrite. Lithics are angular and both high and low resisitvity. Some low resistivity lithics have a high resistivity halo.
B: Core of partially-welded Whakamaru Group ignimbrite in well TH12 (Tauhara Geothermal Field).

Figure 3: FMI facies linked to volcanic lithofacies. Each example is compared to field outcrop or equivalent core. All FMI images are dynamically normalised resistivity images. Depths are in mRL.

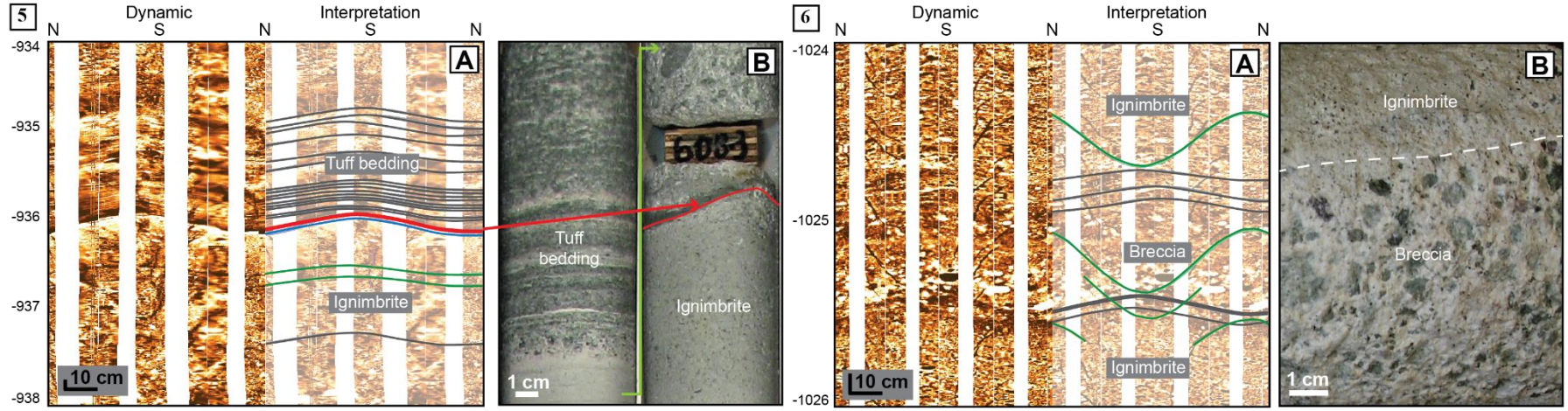

A: FMI image log with low (green sinusoids) and high (blue sinusoid) resistivity fractures, and layers (grey sinusoids). The contact between layers in tuff beds at the base of the Waiora Formation and the top of the Whakamaru Group ignimbrite is shown as a red sinusoid.
B: Contact between tuff beds of the Waiora Formation and the Whakamaru Group ignimbrite in core from well WKM14 (Wairakei Geothermal Field).

A: FMI image log with low resistivity fractures (green sinusoids) and layering (grey sinusoids). The coarse textured breccia may represent a clasts segregation zone in a partially- non-welded part of the ignimbrite. High and low resisitivity lithics are common.
B: Core of coarse texture zone in the Stockyard ignimbrite in well WK247 (Wairakei Geothermal Field), similar to those present in the Whakamaru Group ignimbrite.

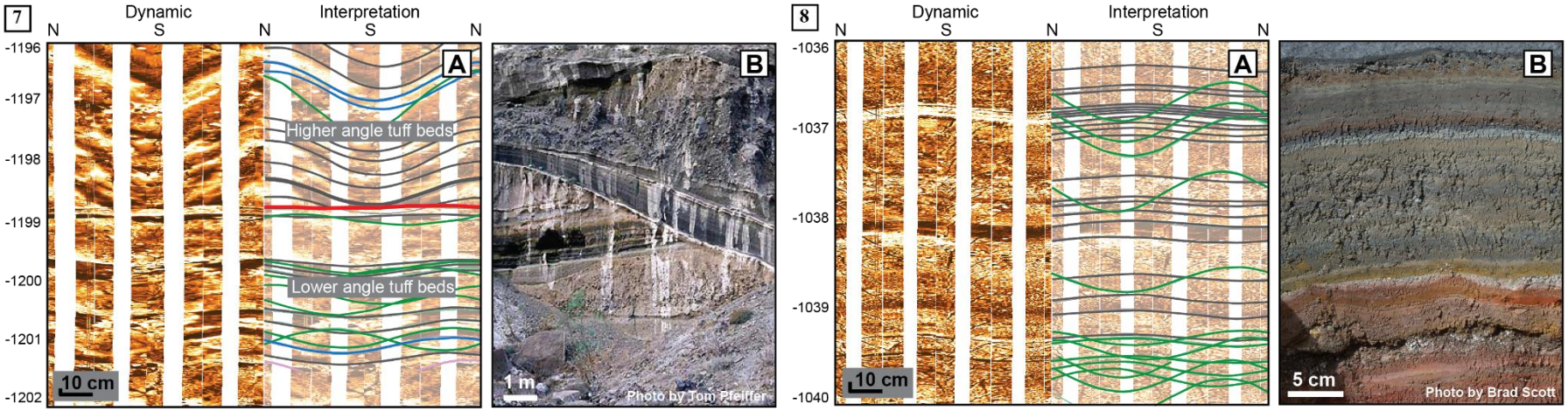

A: FMI image log with low (green sinusoids) and high (blue sinusoids) resistivity fractures and bedding. Higher angle (>75^{o}) tuff beds are truncated against (red sinusoid) lower (>60^{o}) angle tuff beds.
B: Outcrop scale example of cross-cutting relationships between tuff beds.

A: FMI image log with low resistivity fractures (green sinusoids) and layering (grey sinusoids). Layering is between tuff beds.
B: Bedded tuff deposits on White Island, New Zealand (non-fractured).

Figure 3: Continued.

Layering in bedding intervals between the WGI flow units is predominantly shallow dipping (76% have dip magnitudes ≤40º) to the SE, though there is a subordinate population of steeply dipping layers (19% have dip magnitudes ≥70º, all present in tuff beds from -1181.5 to -1224.8 mRL), dipping to the S (Figure 4A).

The cumulative dip-azimuth vector plot is constructed using the dip directions of ignimbrite layers, which highlights changes in layer orientation trend and is used to divide the WGI flows into three zones with consistent dip orientation (Figure 4B,C). There are no lithologies present that could be assumed to have been deposited horizontally, such as would be the case for mudstone in sedimentary basins, so the structural dip of the succession could not be assessed. Therefore, all layering has been assumed to reflect depositional dips with no tectonic tilt component. This assumption is in agreement with Wilson et al. (1986), who states that the WGI generally have undergone little or no tilting since their emplacement. Layers in the top 151 and basal 30 m dip towards the SW, with the middle 165 m dipping to the SSE (Figure 4C). Overall, layering within the WGI has a relatively shallow dip (87% have dip magnitudes ≤40º, and 44% are ≤20º) to the SW (Figure 4A).

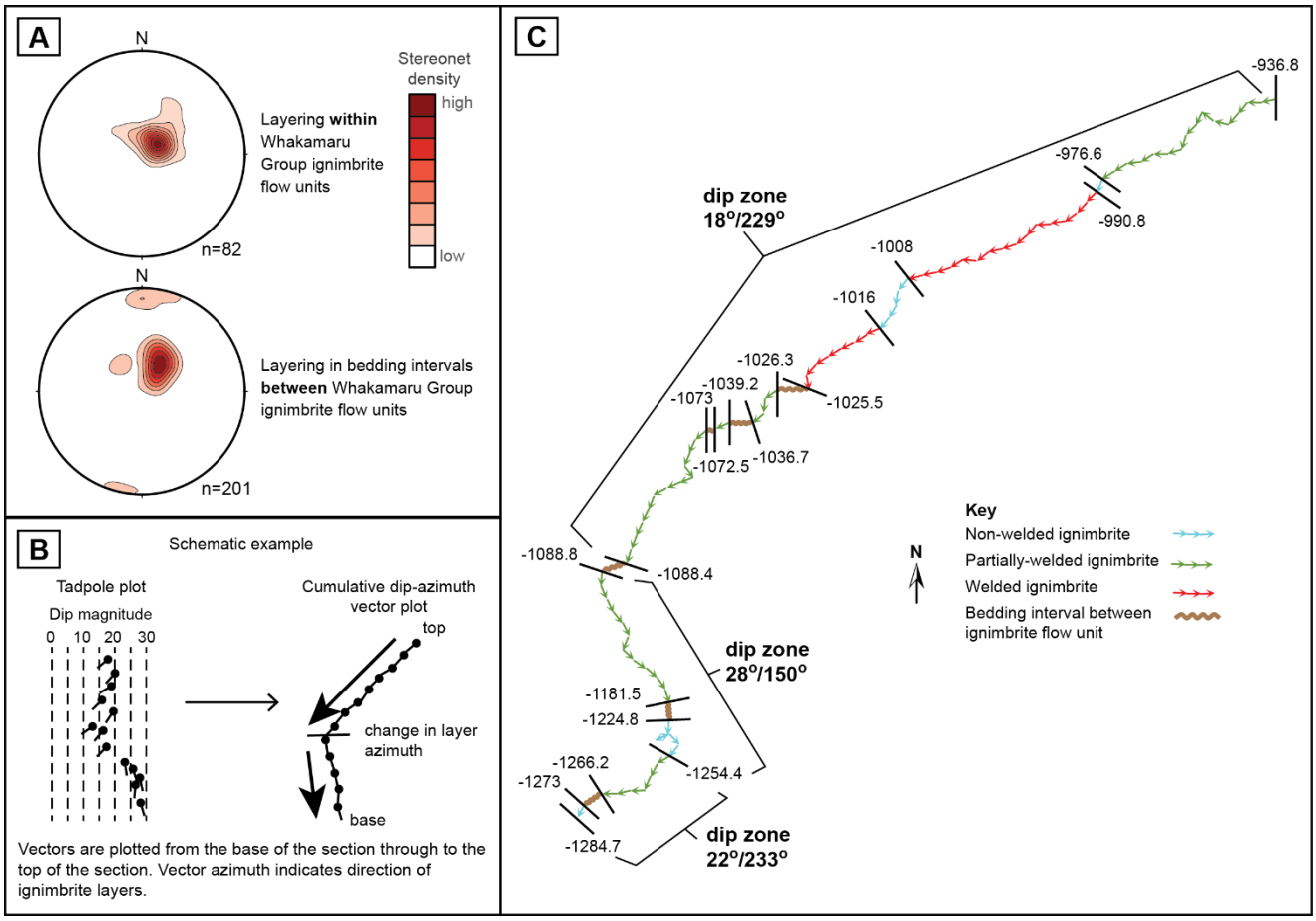

Figure 4: A) Contoured, lower hemisphere stereonets of poles to planes show layering orientation for Whakamaru Group ignimbrite in WK271. Stereonets contoured using Fisher Distribution with color scales representing percentages (Grohmann and Campanha, 2010). Contours are of data corrected for orientation bias, n = raw data set (uncorrected for orientation sample bias). B) Schematic example of the construction of a cumulative dip-azimuth plot from data in a tadpole plot. C) Cumulative dip-azimuth vector plot of layering in the Whakamaru Group ignimbrite colored by rock facies. The average dip magnitude/dip direction is noted for each of the 3 main dip zones. Depths are in mRL.

3.3 Layering and fracture density

Layering and fracture density in the WGI is variable (Figure 5). Fracture density is high in both welded and partially-welded ignimbrite intervals with the lowest density in non-welded intervals. The highest density of layers occurs in intervals of bedding between ignimbrite flow units.

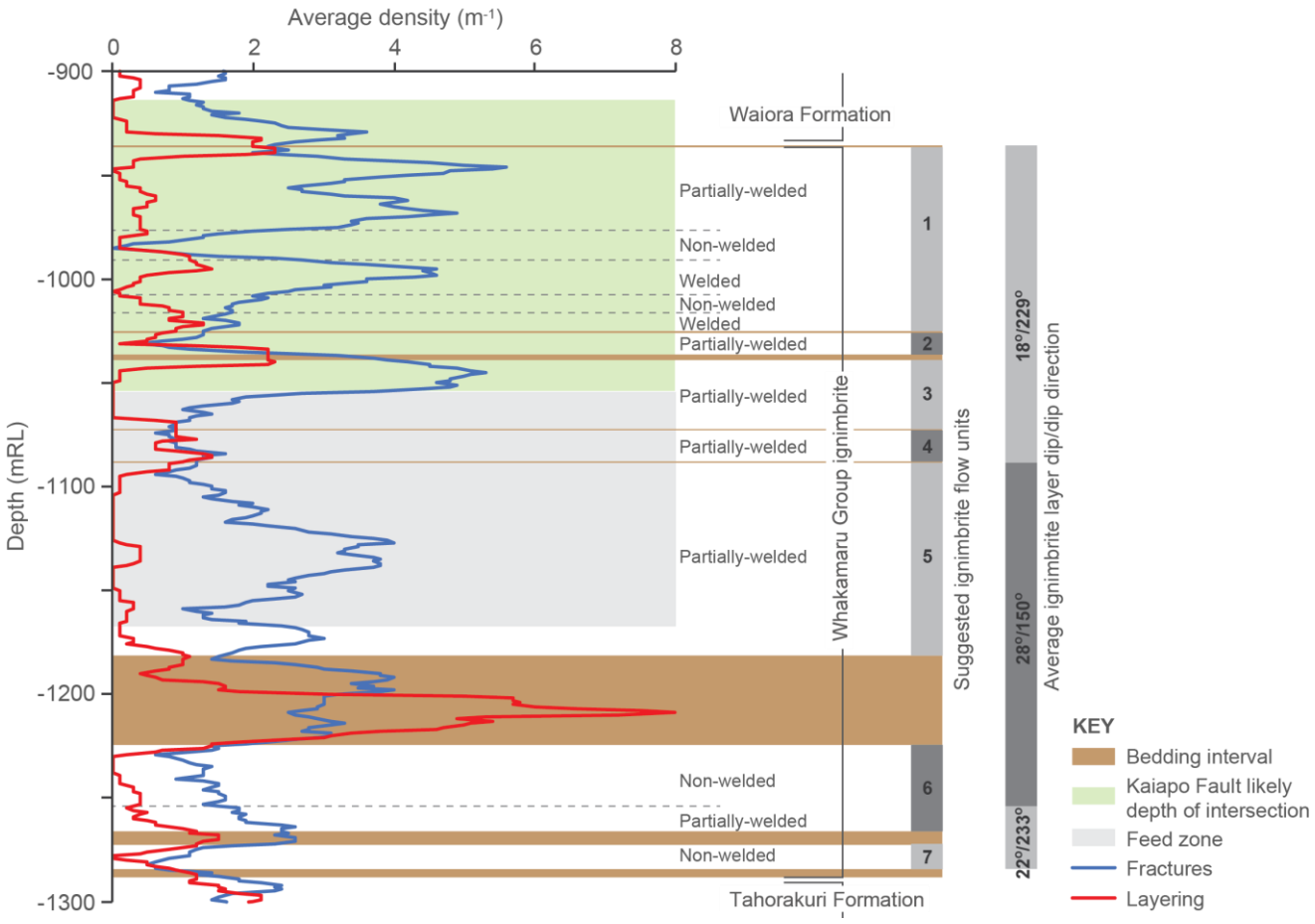

Figure 5: Layering and fracture density (uncorrected for orientation bias) compared to FMI image facies for the Whakamaru Group ignimbrite in well WK271. The plot was generated with a moving average of fracture and layering data with a window of 10 m and a step of 1 m. The zone of potential intersection of the Kaiapo Fault in the well is indicated, along with a major feed zone identified in Massiot et al. (2017). Suggested ignimbrite flow units and the average ignimbrite layer dip/dip direction (from Figure 4C) are indicated.

4. DISCUSSION

4.1 Resistivity response of the Whakamaru Group ignimbrite

Variation in relative resistivity in FMI image logs is due to variations of mineralogy, porosity, and fluid content (Galliot et al., 2007), making FMI logs well suited to imaging planar features and more capable of revealing characteristic like foliation, layering, or systematic variations in resistivity related to mineralogy or fluids than BHTV logs (Davatzes and Hickman, 2005). The dominant resistivity responses of textural and bedding components of the WGI observed are presented in Table 1.

Table 1: Resistivity response from various volcanic components.

Image component	Dominant alteration mineral	Low resistivity	High resistivity
Pumice		✓	
Lithic	Clay	✓	
Lithic	Quartz		✓
Primary quartz			✓
Tuff bed		✓	✓

Hydrothermal alteration minerals can also influence the resistivity response. The imaged interval in well WK271 has a high-temperature alteration assemblage present, with moderate to strong alteration to illite, chlorite, quartz, epidote, pyrite and trace calcite. Of these minerals, clay and quartz are the most abundant and have the highest impact on resistivity response. Clay (both illite and chlorite) will

provide low resistivity response and quartz a high resistivity response (Halwa et al., 2013). Where lithics are altered to either clays or quartz, they will appear either conductive or resistive with respect to the resistivity response of the surrounding rock (Figure 3.4). Given the silicic nature of pumice, normally associated with high resistivity response, the alteration of pumice to clays could account for the low resistivity response observed. This is consistent with a high degree of clay alteration observed in drill cuttings. Further comparison of core and image log, not available to date in the TVZ, would confirm these interpretations.

In addition to the presence of quartz as an alteration mineral, primary volcanic quartz is a common component (>30 vol.%) of the WGI and can be characteristically large (up to 5 mm; Rosenberg, 2017). Common high resistivity, small fragments exhibited in some of the imaged intervals (Figure 3.3) may be attributed to these crystals.

The effect of fluid content on resistivity response is mixed. Pumice can be porous (high fluid) in non-welded ignimbrite (Figure 3.1) or relatively non-porous (low fluid) in partially-welded (Figure 3.3 & 3.4) to welded ignimbrite (Figure 3.2), but seems to have consistently a low resistivity response. Fluid content appears to have more impact in the resistivity response of tuff beds. These have contrasting high and low resistivity beds, which assuming a relatively consistent mineralogy and componentry, might be due to porosity and hence fluid content variations (Figure 3.5, 3.7 & 3.8). It is also possible that variation in grain size would be sufficient to account for the different resistivity response.

4.2 Lithological analysis

The interpreted WGI flow units are delineated by zones of closely spaced layers (Figure 3.7 & 3.8), interpreted as tuff beds formed during short periods of less intense eruptive phases occurring between the emplacement of ignimbrite units. These periods of airfall support the theory that the WGI has multiple subdivisions (Briggs, 1976). Using the tuff beds as markers between the larger ignimbrite emplacement events, the WGI in this part of the Wairakei Geothermal Field can be divided into at least seven flow units (Figure 5). The 89 m-thick shallowest flow unit could possibly represent several flow units based on variable welding, though as these are not separated by tuff beds, they are not differentiated. The observed truncation of some of these tuff beds on the FMI image, and their high angle appearance (Figure 3.7), suggest possible intervals of landscape incision in the times between the ignimbrite forming eruptions and subsequent topographic draping of airfall (McPhie et al., 1993).

The detailed interpretation of ignimbrite welding intensity in the WGI shows that fracture density is low in non-welded intervals (Figure 5). Partial-welded and welded intervals have a higher, but variable fracture density. Low fracture density could be used as an interpretive tool in image logs to identify potential non-welded ignimbrite intervals, where the refinement of welding intensity is not possible from cuttings alone.

Ignimbrite layer dip azimuths, illustrated using a cumulative dip-azimuth vector plot, (Figure 4C) are bimodal. Azimuths through 181.9 m of the total imaged thickness dip SW and 165.6 m dip SSE, possibly supporting flows originating at two eruptive sources within the Whakamaru Caldera (Figure 1) to the NE and NNW, respectively. Some of the layering in the ignimbrite is attributed to post-depositional welding and devitrification processes (McPhie et al., 1993), which would therefore give no indication of flow direction. However, given the consistence of layering dip directions between multiple inferred flow units, we conclude that they provide a good indication of ignimbrite flow direction, though the possibility remains that this could be a local flow direction controlled by pre-existing topography.

4.3 Assessment of intrinsic permeability in the Whakamaru Group ignimbrite

In the case of the WGI in well WK271, there is no systematic link between layer density and the major feed zone (Figure 5) delineated by Massiot et al. (2017). The density of layers in the feed zone is generally lower that the rest of the WGI interval, suggesting that at least in this case, layering in the ignimbrite is not providing significant pathways for fluid flow. However, the Kaiapo Fault intersects the well in the WGI. The Kaipo Fault intersection in well WK271 is based on 3D geological modelling (Alcaraz, 2014) utilizing stratigraphic offsets and detailed LiDAR surface fault mapping (Villamor et al., 2015), but the precise depth is unconstrained due to the similar borehole trend and fault dip direction. Work by Massiot et al. (2017) shows that fractures of low resistivity displaying a high resistivity halo (Figure 6) are dominantly located within the feed zones. The feed zone in Figure 5 contains 43% of all fractures with halo identified in the well, even though this interval covers only 13% of the total imaged well length. Based on the low density of layers in the feed zone, we concur with Massiot et al. (2017), who suggested that fractures with haloes may be related to the damage zone of the Kaiapo Fault and provide flow pathways. Some of the fluid flow may be controlled by intrinsic permeability and flow along layers, but in this case, the contribution is masked by significant flow associated with fractures. Further lithological interpretation of FMI logs in areas away from an active fault zone would clarify the role of layering in providing flow pathways.

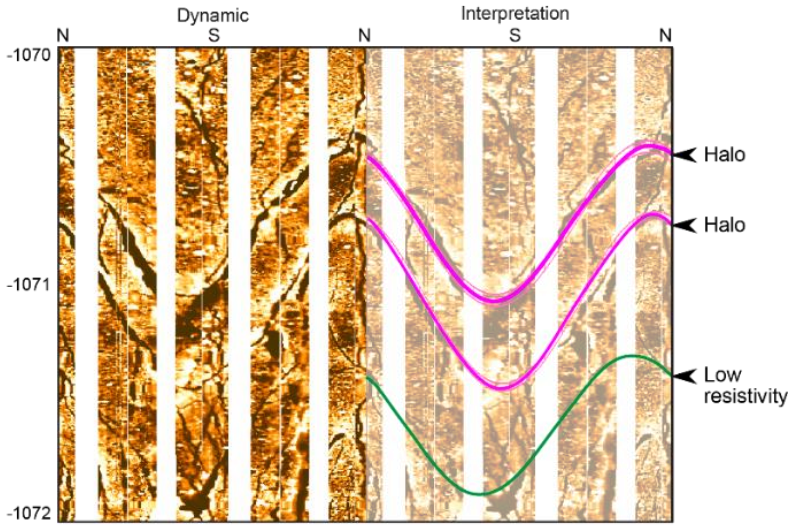

Figure 6: Dynamically normalised resistivity image log in well WK271 of fractures showing examples of permeable fractures with haloes (pink sinusoids) and a low resistivity fracture (green sinusoid). After Massiot et al. (2017).

5. CONCLUSIONS

The resistivity image log interpretation of well WK271 in the Wairakei Geothermal Field has allowed a high-resolution investigation into volcanic textures within the WGI that were previously unknown or otherwise inaccessible. The FMI textural interpretation improves resolution of the stratigraphic sequence, unable to be determined by examination of drill cuttings. This has provided additional insight into the volcanic products of one of the large caldera forming eruptive sequences in the TVZ, with the identification of at least seven discrete flow units, separated by fine-grained layers thought to represent short-lived, less-intense, eruptive phases.

Analysis of FMI from the WGI in well WK271 suggests fluid flow contributions from intrinsic permeability in the ignimbrite units is low, or masked by the likely significant contributions from fracturing associated with the damage zone of the proximal Kaiapo Fault which intersects this well with the WGI interval.

Volcanological, textural, and lithological interpretation from FMI logs, in addition to the usual structural interpretations, are proven here to be critical inputs into conceptual and numerical models of a geothermal system, and stand to improve resolution of 3D geological models.

ACKNOWLEDGEMENTS

This study is part of GNS Science's *New Zealand Geothermal Future* research programme, funding of which was provided by the Government of New Zealand. We thank Contact Energy Ltd. for the provision and permission to publish well data. The authors acknowledge support of this work by Haliburton Software and Services, a Haliburton Company, through the use of Recall™ Borehole software. Thanks to Fabian Sepulveda, Mark Lawrence, and Michael Rosenberg for valuable discussion and editorial comments.

REFERENCES

Alcaraz, S.A.: Update to the Wairakei-Tauhara 3-D geological model. GNS Science consultancy report 2014/113LR (2014).

Bartetzko, A., Paulick, H., Iturrino, G. and Arnold, J.: Facies reconstruction of a hydrothermally altered dacite extrusive sequence: evidence from geophysical downhole logging data (ODP Leg 193). *Geochemistry, Geophysics, Geosystems*, **4** (2003).

Batir, J., and Davatzes, N.C.: Preliminary model of fracture and stress state in the Hellisheidi Geothermal Field, Hengill Volcanic System, Iceland. *Proceedings*, 37th Workshop on Geothermal Reservoir Engineering, Stanford University, Stanford, CA (2012).

Begg, J.G. and Mouslopoulou, V.: Analysis of late Holocene faulting within an active rift using lidar, Taupo Rift, New Zealand. *Journal of Volcanology and Geothermal Research*, **190**, 152-167 (2010).

Bignall, G., Milicich, S.D., Ramirez, L E., Rosenberg, M.D., Kilgour, G.N., and Rae, A. J.: Geology of the Wairakei-Tauhara geothermal system, New Zealand. *Proceedings*, Worlds Geothermal Congress, Bali, Indonesia (2010).

Bignall, G., Rae, A. and Rosenberg, M.: Rationale for targeting fault versus formation-hosted permeability in high-temperature geothermal systems of the Taupo Volcanic Zone, New Zealand. *Proceedings*, World Geothermal Congress, Bali, Indonesia (2010).

Branney, M.J., and Kokelaar, B.P.: Pyroclastic density currents and the sedimentation of ignimbrites. Geological Society of London, (2002).

Briggs, N.D.: Recognition and correlation of subdivisions within the Whakamaru Ignimbrite, central North Island, New Zealand. *New Zealand Journal of Geology and Geophysics*, **19**, 463-501 (1976).

Brown, S.J.A., Wilson, C.J.N., Cole, J.W., and Wooden, J.: The Whakamaru group ignimbrites, Taupo Volcanic Zone, New Zealand: evidence for reverse tapping of a zoned silicic magmatic system. *Journal of Volcanology and Geothermal Research*, **84**, 1-37 (1998).

Browne, P.R.L.: Petrological logs of drillholes, Broadlands geothermal field. *New Zealand Geological Survey*, Report 52 Lower Hutt (1971).

Davatzes, N.C., and Hickman, S. H.: Comparison of acoustic and electrical image logs from the Coso geothermal field, CA. *Proceedings*, 30th Workshop on Geothermal Reservoir Engineering, Stanford University, Stanford, CA (2005).

Davatzes, N. C., and Hickman, S. H. (2009). Fractures, stress and fluid flow prior to stimulation of well 27-15, Desert Peak, Nevada, EGS Project. *Proceedings*, 34th Workshop on Geothermal Reservoir Engineering, Stanford University, Stanford, CA (2009).

Davatzes, N., and Hickman, S. H.: Stress, fracture, and fluid-flow analysis using acoustic and electrical image logs in hot fractured granites of the Coso geothermal field, California, U.S.A. In M. Pöppelreiter, Garcia-Carballido and Kraaijveld (eds.), *Dipmeter and Borehole Image Log Technology*, American Association of Petroleum Geologists Memoir 92, Tulsa OK, 259-294 (2010).

Downs, D.T., Rowland, J.V., Wilson, C.J.N., Rosenberg, M.D., Leonard, G.S., and Calvert, A.T.: Evolution of the intra-arc Taupo-Reporoa Basin within the Taupo Volcanic Zone of New Zealand. *Geosphere*, **10**, 185-206 (2014).

Eastwood, A.A., Gravley, D.M., Wilson, C.J.N., Chambefort, I., Oze, C., Cole, J.W., and Ireland, T.R.: U-Pb dating of subsurface pyroclastic deposits (Tahorakuri Formation) at Ngatamariki and Rotokawa geothermal fields, *Proceedings*, 35th New Zealand Geothermal Workshop, Rotorua, New Zealand (2013).

Galliot, P., Brewer, T., Pezard, P., and Yeh, E.: Borehole imaging tools – principles and applications. *Scientific Drilling*, **5**, 1-4 (2007).

Genter, A., Traineau, H., Dezayes, C., Elsass, P., Ledesert, B., Meunier, A., and Villemin, T.: Fracture analysis and reservoir characterization of the granitic basement in the HDR Soultz Project (France). *Geothermal Science and Technology*, **4**, 189–214 (1995).

Grant, M.A., and Bixley, P.F.: Geothermal Reservoir Engineering (2nd ed.). Burlington, USA: Academic Press (2011).

Grindley, G.W.: Sheet 8—Taupo. Geological map of New Zealand 1: 250 000. Department of Scientific and Industrial Research, Wellington, New Zealand (1960).

Grohmann, C.H., and Campanha, G.A.C.: OpenStereo: Open source, cross-platform software for structural geology analysis. Abstract IN31C-06 presented at 2010 Fall Meeting, AGU, San Francisco, California (2010).

Halwa, L., Wallis, I.C., and Lozada, G.T.: Geological analysis of the volcanic subsurface using borehole resistivity images in the Ngatamariki Geothermal Field, New Zealand. *Proceedings*, 35th New Zealand Geothermal Workshop (2013).

Healy, J., Schofield, J.C., and Thompson, B.N.: Geological map of New Zealand 1:250,000 Sheet 5 Rotorua. Department of Scientific and Industrial Research, Wellington, New Zealand (1964).

Hurley, N.F.: Recognition of faults, unconformities, and sequence boundaries using cumulative dip plots. *American Association of Petroleum Geologists Bulletin*, **78**, 1173-1185 (1994).

Langridge, R.M., Ries, W.F., Litchfield, N.J., Villamor, P., Van Dissen, R.J., Barrell, D., Langridge R.M., Rattenbury, M.S., Heron, D.W., Haubrock, S., Townsend, D.B., and Lee, J.M.: The New Zealand active faults database. *New Zealand Journal of Geology and Geophysics*, **59**, 86–96 (2016).

Leonard, G.S., Begg, J.G., and Wilson, C.J.N. (compilers): Geology of the Rotorua area: scale 1:250,000. Institute of Geological & Nuclear Sciences 1:250,000 geological map 5. Institute of Geological & Nuclear Sciences Limited, Lower Hutt, New Zealand (2010).

Lofts, J.C., and Bourke, L.T.: The recognition of artefacts from acoustic and resistivity borehole imaging devices. *Geological Society, London*, Special Publications, **159**, 59–76 (1999)

Martin, R.C., 1965. Lithology and eruptive history of the Whakamaru ignimbrites in the Maraetai area of the Taupo volcanic zone, New Zealand. *New Zealand Journal of Geology and Geophysics*, **8**, 680-705.

Massiot, C., McNamara, D.D., and Lewis, B.: Interpretive review of the acoustic borehole image logs acquired to date in the Wairakei-Tauhara Geothermal Field. GNS Science report 2013/04 (2013).

Massiot, C., McNamara, D.D., and Lewis, B.: Processing and analysis of high temperature geothermal acoustic borehole image logs, New Zealand, *Geothermics*, **53**, 190–201 (2015).

Massiot, C., McLean, K., McNamara, D.D., Sepulveda, F., and Milicich, S.D.: Discussion between a reservoir engineer and a geologist: permeability identification from completion test data and borehole image logs integration. *Proceedings*, 39th New Zealand Geothermal Workshop, Rotorua, New Zealand (2017).

McLean, K., and McNamara, D.D.: Fractures interpreted from acoustic formation imaging technology: correlation to permeability. *Proceedings*, 36th Workshop on Geothermal Reservoir Engineering, Stanford University, Stanford, CA (2011).

McNamara, D.D., Massiot, C., and Milicich, S.D.: Characterising the subsurface structure and stress of New Zealand's geothermal fields using borehole images, *Energy Procedia*, **125**, 273-282 (2017).

McNamara, D.D, and Massiot, C.: Geothermal structural geology in New Zealand: innovative charcterisation and micro-analytical techniques. *Proceedings*, 38th New Zealand Geothermal Workshop, New Zealand (2016).

McNamara, D.D., Bannister, S., Villamor, P., Sepulveda, F., Milicich, S., Alcaraz, S., and Massiot, C.: Exploring structure and stress from depth to surface in the Wairakei Geothermal Field, New Zealand. *Proceedings*, 41st Workshop on Geothermal Reservoir Engineering, Stanford University, Stanford, CA (2016).

McPhie, J., Doyle, M., Allen, R.: Volcanic textures – a guide to the interpretation of textures in volcanic rocks. Centre for Ore Deposit and Exploration Studies, University of Tasmania (1993).

Risk, G.F.: Electrical resistivity survey of the Wairakei geothermal field. *Proceedings*, 6th New Zealand Geothermal Workshop, Auckland, New Zealand, 123–128 (1984).

Rosenberg, M.D., Bignall, G., and Rae, A.J.: The geological framework of the Wairakei–Tauhara geothermal system, New Zealand. *Geothermics*, **38**, 72-84 (2009).

Rosenberg, M.: Volcanic and tectonic perspectives on the age and evolution of the Wairakei-Tauhara geothermal system. PhD, Voctoria University of Wellington, New Zealand (2017).

Terzaghi, R.D.: Sources of error in joint surveys. *Geotechnique*, **15**, 287–304 (1965).

Villamor, P., Clark, K., Watson, M., Rosenberg, M. D., Lukovic, B., Ries, W., and González, Á.: New Zealand geothermal power plants as critical facilities: an active fault avoidance study in the Wairakei Geothermal Field, New Zealand. *Proceedings*, World Geothermal Congress, Melbourne, Australia, 19–25 (2015).

Watton, T.J., Cannon, S., Brown, R.J., Jerram, D.A. and Waichel, B.L.: Using formation micro-imaging, wireline logs and onshore analogues to distinguish volcanic lithofacies in boreholes: examples from Palaeogene successions in the Faroe–Shetland Basin, NE Atlantic. *Geological Society, London, Special Publications*, **397**, 173-192 (2014).

Wilson, C.J.N., Houghton, B.F., and Lloyd, E.F.: Volcanic history and evolution of the Maroa-Taupo area, central North Island. In I.E.M. Smith (ed), Late Cenozoic volcanism in New Zealand. *Royal Society of New Zealand Bulletin*, **23**, 194-223 (1986).

Wilson, C.J.N., Houghton, B.F., McWilliams, M.O., Lanphere, M.A., Weaver, S.D., and Briggs, R.M.: Volcanic and structural evolution of Taupo Volcanic Zone, New Zealand: a review. *Journal of Volcanology and Geothermal Research*, **68**, 1–28 (1995).

Wilson, C.J.N., and Rowland, J.V.: The volcanic, magmatic and tectonic setting of the Taupo Volcanic Zone, New Zealand, reviewed from a geothermal perspective. *Geothermics*, **59**, 1–20 (2016).